Polarized proton capture on ^{30}Si

C. P. Cameron, R. D. Ledford, M. Potokar,* D. G. Rickel, N. R. Roberson, and H. R. Weller
Physics Department, Duke University, Durham, North Carolina 27706
and Triangle Universities Nuclear Laboratory, Duke Station, Durham, North Carolina 27706

D. R. Tilley
Physics Department, North Carolina State University, Raleigh, North Carolina 27607
and Triangle Universities Nuclear Laboratory, Duke Station, Durham, North Carolina 27706
(Received 26 December 1979)

The 90° yield curves for the ^{30}Si$(p,\gamma_0)^{31}$P and ^{30}Si$(p,\gamma_1)^{31}$P reactions have been measured for $E_p = 5.0$ to 28.0 MeV. Angular distributions of cross section and analyzing power were obtained at twelve energies between $E_p = 6.36$ and 14.45 MeV. The cross sections were measured at nine angles between 30° and 154°, the analyzing power at seven angles between 42° and 142°. For the case of $(\vec{p},\gamma_0)$ the complex T-matrix elements were extracted, assuming that the angular distributions are governed by coherent $E1$ and $E2$ processes. Two $\sigma(E2)$ yield curves are obtained, one of which exhausts 9–12% of the $\Delta T = 0$ $E2$ energy weighted sum rule while the other exhausts 21–31%. The results are compared to direct-semidirect model calculations which suggest that the larger $E2$ cross sections are the physical solutions.

[NUCLEAR REACTIONS ^{30}Si$(\vec{p},\gamma_0)$ ^{30}Si$(\vec{p},\gamma_1)$ measured $\sigma(\theta)$ and $A(\theta)$, $E_p = 6.4$ to 15.0 MeV. ^{30}Si(p,γ_0) ^{30}Si(p,γ_1) measured $\sigma(90°)$, $E_p = 5.0$ to 28.0 MeV. Deduced $E1$ and $E2$ T-matrix amplitudes and phases. Compared to model calculations.]

I. INTRODUCTION

The use of polarized protons has been shown to be an effective tool for understanding the proton capture reaction in the region of the giant dipole resonance.[1-3] In addition, such studies can be used to search for non-$E1$ radiation such as might be expected from the decay of the isoscalar electric giant quadrupole resonance (GQR) which is located at excitation energies[4] at or slightly below the GDR. Measurements of angular distributions of cross section and analyzing power are particularly valuable for those cases where the spins of the target and residual nuclei are 0 and $\frac{1}{2}$ (or $\frac{1}{2}$ and 0), since it is then, in principle, possible to obtain the total $E2$ strength from a transition matrix element analysis[1,5,6] with a minimum number of model dependent assumptions.

Previously published polarized capture studies of $E2$ radiation in the region of the GDR have been carried out only in light nuclei: ^{14}C$(p,\gamma_0)^{15}$N (Refs. 6 and 7) and ^{15}N$(p,\gamma_0)^{16}$O (Refs. 8 and 9). For the former case, the extracted integrated $E2$ cross section varies rather smoothly through the region of excitation energies from 14 to 27 MeV and is in reasonable agreement with a direct-semidirect model calculation[10-12] which assumes pure direct $E2$ capture.[7] These results suggest that either the isoscalar GQR in ^{15}N has a small (γ,p_0) branch or that the $E2$ strength is very spread out, or both. The case of proton capture leading to ^{16}O indicates a different behavior. Here $\sigma_{E2}(p,\gamma_0)$ exceeds the calculated direct $E2$ cross section and, when expressed (by detailed balance) as a (γ,p_0) cross section, gives[9] 12 to 22% or 20 to 30% of the isoscalar energy-weighted sum rule (EWSR) when integrated from $E_x = 17.9$ to 27.3 MeV or 13.9 to 29.0 MeV, respectively. However, recent $(\alpha,\alpha'c)$ coincidence measurements[13] of the isoscalar GQR in ^{16}O show only 9% of the same EWSR for $E_x = 17.9$–27.3 MeV in the p_0 channel. Some of the disagreement can be removed by considering the pure isoscalar nature of the (α,α') reaction. A discrepancy still exists between the results of the two measurements. Since the $E2$ strength observed by the (p,γ_0) reaction peaks near $E_x = 25$ MeV, which is higher in excitation energy than the isoscalar $E2$ strength observed in the (α,α') experiment.[13] It has been suggested,[8,9] on the basis of these data, that some of the $E2$ strength observed in the ^{15}N$(p,\gamma_0)^{16}$O reaction may correspond to low-energy fragments of the isovector GQR.

In the present work, angular distributions of cross sections $\sigma(\theta)$ and analyzing powers $A(\theta)$ have been measured for the polarized proton capture reaction ^{30}Si$(p,\gamma_{0,1})^{31}$P$(Q = 7.29$ MeV) for excitation energies which encompass the region of the GDR and the expected region of the GQR.[4] The measurements of $\sigma(\theta)$ were made at 9 angles (30°–154°) and $A(\theta)$ at 7 angles (42°–142°). In addition, the 90° yield curve has been measured for γ_0

and γ_1 for $E_p(E_x) = 5(12.1)$ to $28(34.4)$ MeV. For these measurements the energy step size was 50 keV for $E_p < 16.1$ MeV and 1 MeV for $E_p > 16$ MeV.

The angular distributions were analyzed (assuming only coherent $E1$ and $E2$ radiation) to determine, at each energy, the relative amplitudes and phases of the T-matrix elements contributing to the decay. The extracted relative amplitudes and phases, as well as the $E2$ cross sections, are compared to a direct-semidirect model[7,10-12] calculation which includes both direct and collective $E2$ contributions.[7,14]

II. EXPERIMENTAL DETAILS

The details of the experimental setup used in the present work have been described previously and only the salient facts will be given here.

The γ rays were detected with a 25.4×25.4 cm NaI crystal surrounded with a plastic anticoincidence shield. The shield gain and discriminator settings were adjusted to reject the major portion of the escape peaks as well as > 99% of the cosmic ray counts. The measurement of the efficiency of the detector system has been described previously.[15,16] For measurements of the yield curves the back face of the NaI detector was positioned 82 cm from the target which corresponds to an angular acceptance of 17.6°. For the $\sigma(\theta)$ and $A(\theta)$ measurements from 42° to 142°, the detector was rolled back to 102 cm (14.2°). Finally, for the measurements at 30° and 154° the back face of the detector was at 145 cm. A typical spectrum is shown in Fig. 1 for $E_p = 15$ MeV and $\theta_\gamma = 90°$.

The targets were self-supporting silicon dioxide prepared by evaporation of enriched (>95%) $^{30}SiO_2$ powder mixed with graphite. The target thicknesses were obtained from elastic proton scattering of 1.88 MeV protons at $\theta_p = 135°$ where the cross section for Si(p,p) is essentially Rutherford. Since thick foils were difficult to make, pairs of targets were used during the experiment and were mounted 1.6 mm apart on the target rod. Two pairs were used at various times: a thin pair with a total thickness of 0.51 mg/cm^2 (55% ^{30}Si by mass) and a thicker pair of 1.15 mg/cm^2 (55% ^{30}Si by mass).

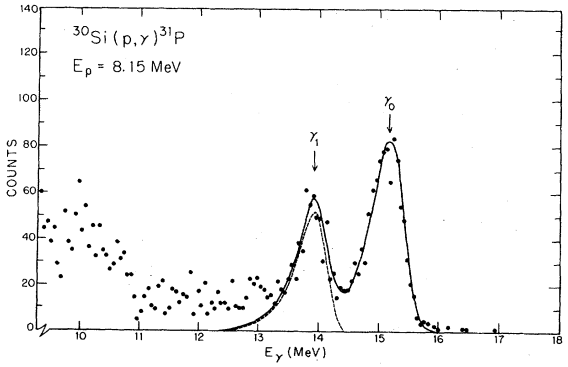

FIG. 1. The high energy portion of the spectrum obtained at $E_p = 8.15$ MeV and $\theta_{lab} = 90°$. The solid curve represents the fit to the two peaks as described in the text. The dashed curve represents the fraction of the fit due only to γ_1.

The polarized proton beam was obtained with the Triangle Universities Nuclear Laboratory (TUNL) Lamb-shift polarized ion source. Beam currents of 30 to 60 nA were available on target. The beam polarization was determined by the quench ratio method.[17] Two 2000 μm silicon detectors were mounted in the scattering chamber at ±160° with respect to the beam direction to monitor the constancy of both the beam polarization and the integrated charge during a given angular distribution measurement. Beam polarizations were typically 0.80 ± 0.02. Beams of unpolarized protons with energies from 16.8 to 28 MeV were obtained from the TUNL Cyclo-Graaff accelerator—a 15 MeV negative hydrogen-ion cyclotron injecting the TUNL FN tandem Van de Graaff. Time-of-flight techniques utilizing the pulsed beam (rf structure) were used to discriminate against the large neutron background, especially at the highest energies.

The total uncertainty in the absolute cross section for this experiment is ±20%. This is due primarily to uncertainties in the target thicknesses and the detector efficiency.

III. DATA ANALYSIS

The yield for the γ-ray transitions to the ground and first excited state was determined by fitting the γ-ray energy spectra with a characteristic line shape and using a least squares criterion. From a preliminary fit to those spectra for which the γ_0 yield was large, it was ascertained that the widths of the full-energy peaks increased with energy in a smooth and systematic way over the energy region studied. All subsequent fits were carried out with a fixed peak width, the width being set at the value corresponding to the appropriate γ-ray energy. The yield in the peak from the γ_1 transitions was obtained by subtracting the fit for γ_0 from the spectrum and then fitting the remaining peak. At energies below 16 MeV, the γ_0 and γ_1 peaks were separated clearly enough for this procedure to be readily performed. At higher bombarding energies where the γ_1 yield is much greater than the yield for γ_0, a simultaneous fit to both peaks was performed with a specified energy separation between the two peaks.

The angular distributions of center of mass cross sections were fitted, using the least squares

criterion, to an expansion of Legendre polynomials:

$$\sigma(\theta)=A_0\left[1+\sum_{k=1}^{4} a_k Q_k P_k(\cos\theta)\right], \quad (1)$$

where the Q_k coefficients correct for the finite geometry. The angular distributions of analyzing powers are given as the product $\sigma(\theta)A(\theta)/A_0$, where

$$A(\theta)=\left(\frac{N_+ - N_-}{N_+ + N_-}\right)\frac{1}{P}, \quad (2)$$

P is the beam polarization, and N_+ and N_- are the yields for spin up and spin down, respectively. These products were fitted to an expansion of associated Legendre polynomials:

$$\sigma(\theta)A(\theta)/A_0=\sum_{k=1}^{4} b_k Q_k P_k^1(\cos\theta)\,. \quad (3)$$

For the (p,γ_0) data, the fits for $\sigma(\theta)$ and $\sigma(\theta)A(\theta)/A_0$ were made through $k=4$. The use of this order in Eq. (1) was statistically justified[18] since the $\sigma(\theta)$ angular distributions were measured, at back angles, out to the zero of $P_5(\cos\theta)$. For Eq. (3), since there is no b_0 and since the zeros of $P_k^1(\cos\theta)$ occur at angles closer to 90° than those of $P_k(\cos\theta)$, accurate b_4's were obtained for the smaller angular range of 42° to 142°. For the (p,γ_1) reaction, $\sigma(\theta)$ was obtained only at seven angles and statistically significant fits could only be made through $k=3$. For the analyzing powers, it was possible to fit through $k=4$, for the reasons discussed above.

IV. RESULTS

A. Yield curves

The 90° yield curves for the decay to the ground state and to the first excited state are shown in Fig. 2. For $E_p \leq 16.1$ MeV the "thin" pair of targets with a combined energy loss of less than 20 keV for 10 MeV protons was used, while for $E_p > 16.8$, the "thick" pair of targets which were ≈ 22 keV thick for 20 MeV protons was used. The upper scales in Fig. 2 are the actual γ-ray energies for the transitions to the ground (γ_0) and first excited (γ_1) states, respectively. These data show evidence for a giant resonance built on the ground state, as well as for one built on the first excited state of ^{31}P.[19]

The photodisintegration reaction ^{31}P$(\gamma,n_0)^{30}$P has been studied by Gellie *et al.*[20] and the total photoneutron cross section by Veyssiere *et al.*[21] Their results along with the ^{31}P(γ,p_0) yield curve, obtained from the present capture work by the use of detailed balance, are shown in Fig. 3. An examination of Fig. 3 shows that the main strength of both the (γ,n_0) and (γ,p_0) reaction lie well below the peak of the total photoneutron cross section, but that some of the structures in the (γ,n_0) and (γ,p_0) yield curves appear to be correlated with the photoneutron cross section. Consequently, it

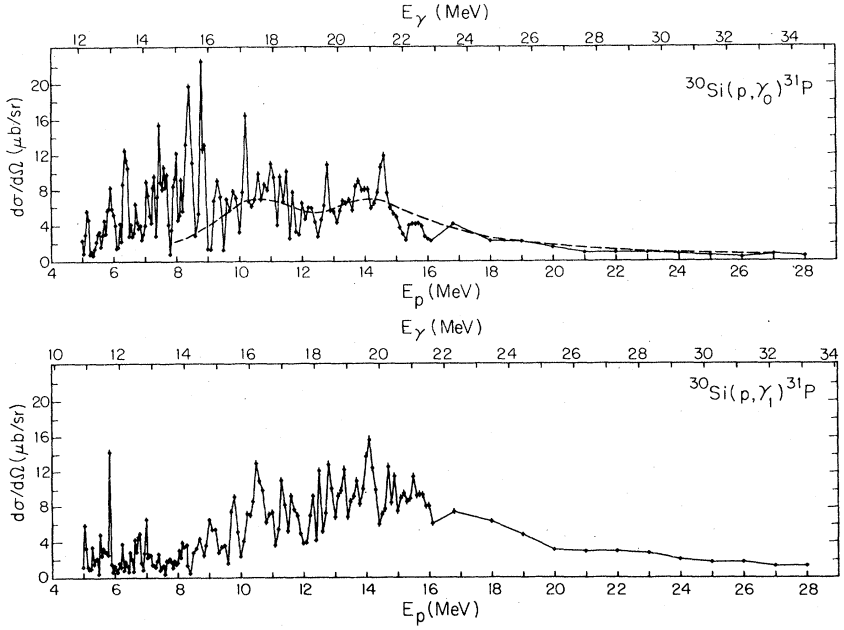

FIG. 2. The differential cross section measured at $\theta_{lab}=90°$ for ^{30}Si$(p,\gamma_0)^{31}$P and ^{30}Si$(p,\gamma_1)^{31}$P ($E_x=1.27$ MeV). The solid curve is a line drawn through the data points. The dashed curve represents the DSD model calculation as described in the text.

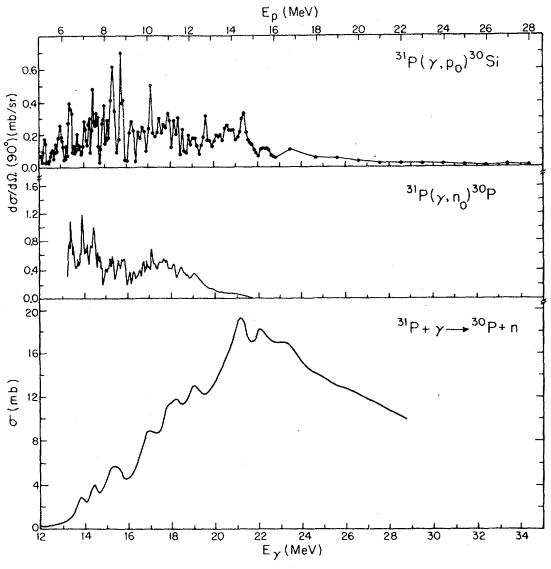

FIG. 3. Comparison of the $^{31}P(\gamma, p_0)$ 90° yield curve obtained in this experiment with the 90° yield curve for the $^{31}P(\gamma, n_0)$ reaction (Ref. 20) and the ^{31}P total photoneutron cross section (Ref. 21). The curves are plotted as a function of E_γ.

appears that the (p,γ_0) reaction is a useful probe for the GDR in ^{31}P, although it is uncertain whether the yield below E_x=16 MeV is primarily from excitation of the GDR.

To compare the $^{31}P(\gamma,p_0)^{30}Si$ yield with the classical dipole sum rule, which is expressed for the $E1$ photon absorption cross section by[22]

$$\int \sigma(E1)dE_\gamma = 60\frac{NZ}{A}\ \text{MeV mb}\,,$$

the 90° cross sections were converted into total cross sections by assuming that the angular distributions vary continuously between the energies at which measurements were made in this experiment (see Sec. IV B below). The resulting (γ,p_0) yield curve was integrated from E_γ=12.0 to 35.0 MeV and gave 21 MeV mb, which is 4.5% of the classical dipole sum rule. A similar procedure was followed for the $^{30}Si(p,\gamma_1)$ reaction and integration of the resulting (γ,p) cross section from E_γ=10.8 to 33.8 MeV gave 24.2 MeV mb; this is 5% of the sum rule.

The phenomenon of isospin splitting of the giant dipole resonance has received considerable attention (Hayward,[22] Akyuz and Fallieros,[23] and Paul[24]). For ^{31}P, a nucleus with $T=\frac{1}{2}$, the giant resonance built upon the ground state may be split into two components: $T=\frac{1}{2}$ and $T=\frac{3}{2}$. The $T_<$ and $T_>$ components may both decay by proton emission to ^{30}Si, but if isospin mixing is negligible, only the $T_<$ component should decay by neutron emission to the $T=0$ ground state of ^{30}P.

Simple expressions have been given for the relative strengths and splitting of the $T_<$ and $T_>$ component of the GDR. One estimate of the splitting (Ref. 23) is

$$\Delta E \equiv \frac{60(T_0+1)}{A}\ \text{MeV}\,,$$

where T_0 is the isospin of the ground state. The relative strength of the two isospin components has been shown to be given by[23]

$$\frac{S(T_0+1)}{S(T_0)} \equiv \frac{1}{T_0}\left[\frac{1-1.5(T_0/A^{2/3})}{1+1.5(1/A^{2/3})}\right].$$

For the present case $\Delta E \sim 2.9$ MeV and $S(T_0+1)/S(T_0)\sim 2.5$. It should be noted that the predicted relative strengths are for the total photon absorption cross sections and may not apply to the (γ,p_0) channel alone.

Above 16 MeV excitation energy, the $^{31}P(\gamma,p_0)^{30}Si$ yield (see Fig. 3) suggests the presence of two broad peaks centered near 17.7 and 21 MeV, the latter being conspicuously absent in the (γ,n_0) data. These two regions were integrated for both $^{31}P(\gamma,p_0)$ and $^{31}P(\gamma,n_0)$. It was assumed that $a_2\approx 0.8$ and $a_4\approx 0$ (see below) for the (γ,p_0) yield, while for (γ,n_0) the angular dependence[25] of the yield was taken as $\sin^2\theta$. The results for these ratios of the strengths are 0.86 and 0.16 for the (γ,p_0) and (γ,n_0) reactions, respectively, suggesting that these two regions (16–19.4 and 19.4–23 MeV) are associated with the $T_<$ and $T_>$ components of the GDR.

B. Angular distributions

A sample of the angular distribution data is shown in Fig. 4 and Fig. 5 for the transitions leading to the ground and first excited state, respectively. The solid curves are the previously described fits. The a_k and b_k coefficients obtained from all the fits are tabulated for (p,γ_0) and (p,γ_1) in Tables I and II, respectively.

The ground state spin of ^{31}P is $\frac{1}{2}^+$ so that the GDR can have $J^\pi=\frac{1}{2}^-$ and $\frac{3}{2}^-$ and the GQR can have $J^\pi=\frac{3}{2}^+$ and $\frac{5}{2}^+$. Since the target has spin 0^+, the excitation of these states requires incoming protons with $(j,\pi_p=(-1)^l)=(J,\pi)$, where l is the orbital angular moment of the incoming proton. For the $^{30}Si(p,\gamma_0)$ reaction, we can write the complex transition matrix elements (in jj coupling) in terms of a real amplitude and a phase as

$$p_{1/2}(E1)e^{i\phi(p_{1/2})}, p_{3/2}(E1)e^{i\phi(p_{3/2})},$$

$$d_{3/2}(E2)e^{i\phi(d_{3/2})}, d_{5/2}(E2)e^{i\phi(d_{5/2})}.$$

While $M1$ radiation could also be present, the $M1$ giant resonance is expected to lie below the excitation region studied in this experiment and to exhaust a large fraction of the $M1$ sum rule.[26]

Consequently only $E1$ and $E2$ radiation were considered in the analysis described below. The expressions relating the T-matrix elements to the a_k and b_k coefficients are as follows:

$$1 = p_{1/2}^2 + 2p_{3/2}^2 + 2d_{3/2}^2 + 3d_{5/2}^2 \text{ (normalization)},$$

$$a_1 = +3.464 p_{1/2} d_{3/2} \cos(p_1, d_3) + 0.693 p_{3/2} d_{3/2} \cos(p_3, d_3) + 6.235 p_{3/2} d_{5/2} \cos(p_3, d_5),$$

$$a_2 = -p_{3/2}^2 - 2p_{1/2} p_{3/2} \cos(p_1, p_3) + d_{3/2}^2 + 0.857 d_{3/2} d_{5/2} \cos(d_3, d_5) + 1.714 d_{5/2}^2,$$

$$a_3 = -3.464 p_{1/2} d_{5/2} \cos(p_1, d_5) - 4.157 p_{3/2} d_{3/2} \cos(p_3, d_3) - 2.771 p_{3/2} d_{5/2} \cos(p_3, d_5),$$

$$a_4 = -6.857 d_{3/2} d_{5/2} \cos(d_3, d_5) - 1.714 d_{5/2}^2,$$

$$b_1 = -1.732 p_{1/2} d_{3/2} \sin(p_1, d_3) - 1.386 p_{3/2} d_{3/2} \sin(p_3, d_3) + 3.118 p_{3/2} d_{5/2} \sin(p_3, d_5),$$

$$b_2 = -p_{1/2} p_{3/2} \sin(p_1, p_3) + 0.714 d_{3/2} d_{5/2} \sin(d_3, d_5),$$

$$b_3 = -1.155 p_{1/2} d_{5/2} \sin(p_1, d_5) + 1.386 p_{3/2} d_{3/2} \sin(p_3, d_3) - 0.231 p_{3/2} d_{5/2} \sin(p_3, d_5),$$

$$b_4 = -1.714 d_{3/2} d_{5/2} \sin(d_3, d_5),$$

where $(p_1, p_3) = \phi(p_{1/2}) - \phi(p_{3/2})$, etc. The unknowns in these equations are the four amplitudes and three relative phases (since one phase can be chosen arbitrarily). There are, therefore, seven unknowns and nine equations.

To find the possible solutions for the amplitudes and relative phases a procedure was used in which these quantities were fitted directly to the experimental cross sections and analyzing powers by minimizing χ^2, expressed as

$$\chi^2 = \sum_{\text{data}} \left(\frac{1}{\Delta\sigma_i}\right)^2 \left[\sigma_i - \sum_k a_k(\text{calc}) Q_k P_k(\cos\theta)\right]^2$$

$$+ \sum_{\text{data}} \left(\frac{1}{\Delta\sigma_i A_i}\right)^2 \left[\sigma_i A_i - \sum_k b_k(\text{calc}) Q_k P_k^1(\cos\theta)\right]^2,$$

where $\sigma_i = \sigma(\theta_i)/A_0$, $\Delta\sigma_i$ is the statistical error of σ_i, and the summation is over the data points. The quantities a_k(calc) and b_k(calc) are calculated from the equations given above. The minimum of χ^2 was obtained with a gradient search routine,[27] and the errors were derived from the error matrix.

Three classes of solutions were found. Two classes (labeled as sets I and II) correspond to having $\sigma(p_{3/2})$ as the dominant part of the $E1$ cross section, with $\sigma(p_{3/2})/\sigma(E1) \approx 0.7$–$0.9$ and $\sigma(p_{3/2})/\sigma(E1) \approx 0.5$–$0.65$, respectively. Here $\sigma(p_{3/2}) + \sigma(p_{1/2}) = \sigma(E1)$. The third class has $\sigma(p_{1/2})$ dominant with $\sigma(p_{1/2})/\sigma(E1) \approx 0.6$–$0.75$.

In a recent publication from this laboratory[3] the $(\vec{p}, \gamma_0)$ reaction data from several targets having $A = 14$ to 88 were used to extract the relative amplitudes and phases of the $E1$ T-matrix elements. Calculations based on a simple direct-

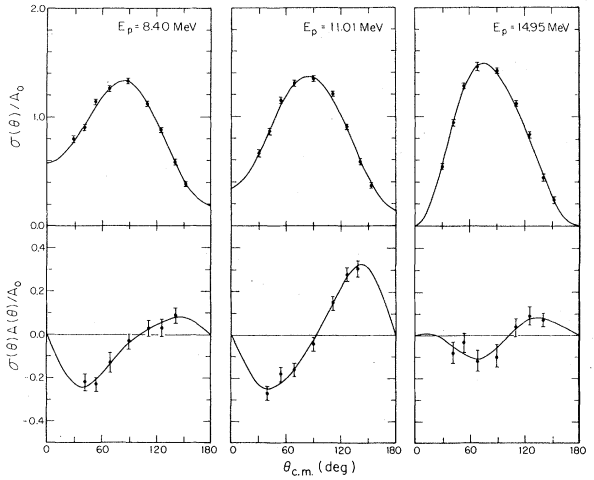

FIG. 4. Typical cross section and analyzing power angular distribution for ^{30}Si$(p, \gamma_0)^{31}$P. The errors are statistical. The solid lines are fits through fourth order in Legendre and associated Legendre polynomials.

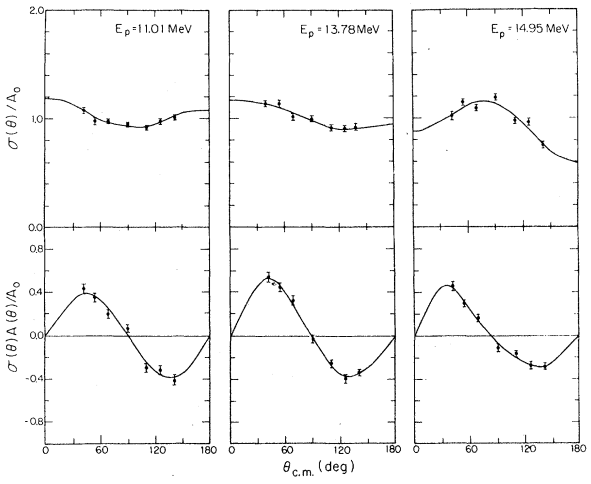

FIG. 5. Same as Fig. 4 for ^{30}Si$(p, \gamma_1)^{31}$P.

TABLE I. The A_0, a_k and b_k coefficients obtained from least squares fits to the $^{30}Si(p,\gamma_0)$ data with Eqs. (1) and (2), respectively. The b_k coefficients are given below the a_k coefficients at each energy. Also given in the two right-hand columns are the χ^2 values obtained when the data were fitted directly to the T-matrix element amplitudes and relative phases as described in the text. The errors given for the A_0 values are statistical.

E_p (MeV)	A_0 (μb/sr)	a_1/b_1	a_2/b_2	a_3/b_3	a_4/b_4	χ^2	χ^2(I) [a]	χ^2(II) [b]
6.36	10.6±0.2	−0.03±0.01	−0.70±0.02	−0.05±0.03	−0.10±0.04	4.0	3.4	3.4
		0.02±0.03	0.03±0.01	0.04±0.01	0.02±0.02	2.4		
7.46	19.6±0.3	0.04±0.01	−0.97±0.02	−0.05±0.03	−0.05±0.04	1.0	0.7	0.7
		−0.09±0.03	−0.02±0.01	0.05±0.02	−0.02±0.02	0.3		
8.40	14.2±0.3	0.19±0.01	−0.64±0.02	−0.00±0.02	0.02±0.03	0.9	0.6	0.6
		−0.07±0.02	−0.10±0.01	−0.02±0.01	−0.01±0.01	0.5		
8.81	13.1±0.3	0.19±0.01	−0.81±0.02	−0.09±0.03	0.06±0.03	1.5	2.2	1.8
		−0.08±0.02	−0.12±0.01	0.02±0.01	0.03±0.01	2.2		
8.85	10.0±0.3	0.24±0.02	−0.69±0.02	−0.15±0.03	−0.05±0.03	1.1	1.2	2.4
		0.01±0.03	−0.07±0.02	−0.03±0.02	−0.00±0.02	1.5		
10.23	10.3±0.2	0.18±0.01	−0.88±0.02	−0.21±0.03	−0.09±0.03	1.0	1.1	1.1
		−0.07±0.02	0.21±0.01	0.07±0.01	0.02±0.01	1.1		
11.01	7.3±0.1	0.15±0.01	−0.74±0.02	−0.04±0.03	−0.03±0.03	0.9	1.0	0.8
		−0.01±0.02	−0.18±0.01	−0.02±0.01	−0.02±0.01	0.9		
12.00	5.7±0.2	0.13±0.01	−0.48±0.02	−0.16±0.03	0.03±0.03	0.7	0.8	1.0
		−0.07±0.03	−0.27±0.02	−0.01±0.02	0.01±0.02	0.8		
12.85	6.6±0.1	0.16±0.01	−0.91±0.02	−0.12±0.03	−0.07±0.03	1.8	1.1	1.1
		0.01±0.02	−0.03±0.01	−0.02±0.01	−0.02±0.01	0.6		
13.78	6.0±0.1	0.13±0.01	−0.81±0.02	−0.16±0.03	0.04±0.03	2.7	2.2	2.7
		−0.03±0.02	−0.07±0.01	0.02±0.01	0.01±0.01	1.9		
14.63	7.3±0.2	0.17±0.01	−0.91±0.02	−0.18±0.03	−0.05±0.03	1.8	1.2	1.2
		0.01±0.02	−0.03±0.01	0.00±0.02	−0.00±0.01	0.6		
14.95	3.6±0.1	0.23±0.01	−0.93±0.02	−0.24±0.03	−0.12±0.04	0.5	0.7	0.7
		−0.03±0.02	−0.05±0.01	0.02±0.02	0.01±0.02	0.7		

[a] Set I, see text.

[b] Set II, see text.

semidirect capture model[10] (see Sec. VI below) were shown to provide a procedure for choosing the physical solutions. For the case of the $^{30}Si(p,\gamma_0)^{31}P$ reaction this calculation indicated that $\sigma(p_{3/2})$ should be the dominant part of the $E1$ cross section with $\sigma(p_{3/2})/\sigma(E1)\approx 0.6$. In fact, the equations for the a_k coefficients indicate that if spin-orbit effects are neglected, so that

TABLE II. The A_0, a_k and b_k coefficients obtained from least squares fits to the $^{30}Si(p,\gamma_1)$ data with Eqs. (1) and (2), respectively. The b_k coefficients are given below the a_k coefficients for each energy. The errors given for the A_0 are statistical.

E_p (MeV)	A_0 (μb/sr)	a_1/b_1	a_2/b_2	a_3/b_3	a_4/b_4	χ^2
10.23	5.3 ±0.1	0.08±0.04	−0.07±0.06	−0.06±0.08		5.4
		0.08±0.03	0.33±0.02	0.01±0.02	−0.03±0.02	2.4
11.01	6.9 ±0.1	0.04±0.03	0.13±0.04	0.01±0.05		1.1
		0.01±0.02	0.27±0.01	0.00±0.01	0.01±0.01	3.7
12.00	4.2 ±0.1	0.19±0.05	0.07±0.07	−0.05±0.10		4.1
		−0.06±0.03	0.26±0.02	0.00±0.02	0.01±0.02	1.7
12.85	10.1 ±0.1	0.16±0.02	−0.26±0.03	−0.05±0.04		1.7
		0.04±0.02	0.25±0.01	0.02±0.01	0.02±0.01	1.8
13.78	7.8 ±0.1	0.15±0.03	−0.06±0.03	−0.04±0.05		1.2
		0.04±0.02	0.31±0.01	0.03±0.01	0.00±0.01	0.7
14.63	6.2 ±0.1	0.21±0.04	0.14±0.05	−0.09±0.08		3.8
		−0.04±0.03	0.20±0.02	0.04±0.02	−0.03±0.02	0.8
14.95	8.49±0.1	0.16±0.02	−0.27±0.03	−0.01±0.04		6.9
		0.01±0.02	0.23±0.01	0.04±0.01	0.03±0.01	1.1

$(p_{3/2})=(p_{1/2})$ and $\phi(p_{3/2})=\phi(p_{1/2})$, the $p_{3/2}$ term will account for $\frac{2}{3}$ of the $E1$ cross section. As will be seen below in Sec. VI, the extended direct-semidirect (DSD) model calculations yield a similar result, but with $\sigma(p_{3/2})$ slightly larger. In the present case these calculations tend to favor the solutions of set II.

The two solutions with $\sigma(p_{3/2})$ dominant, i.e., the solution sets I and II, are shown in Figs. 6 and 7. The values of $\sigma(d_{5/2})$ for both sets I and II tend to lie in the range of 0.5 to 0.8 with set I being slightly higher than those of set II. The $E1$ relative phases $\sigma(p_{1/2})-\phi(p_{3/2})$ are, for the most part, small ($\leq 40°$), as was expected, since the difference is due to the spin-orbit term in the optical-model potential. The same should be true for the relative phases of the $E2$ amplitudes, $\phi(d_{3/2})-\phi(d_{5/2})$; the average trend is in this direction, but there are some rather large deviations.

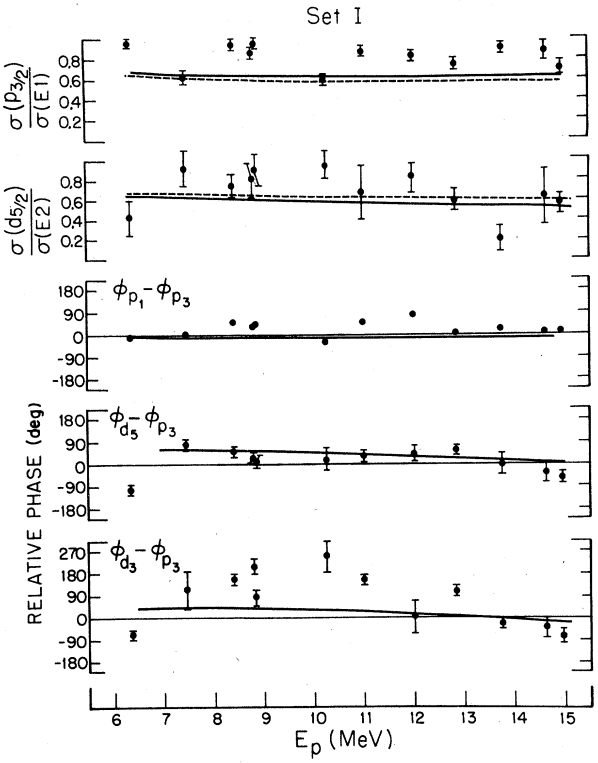

FIG. 6. The results of the $E1$–$E2$ analysis for the ^{30}Si$(\vec{p},\gamma_0)$ reaction for the solutions with $\sigma(p_{3/2})/\sigma(E1)\approx 0.85$. The solid lines are the extended DSD model prediction. The dashed lines are pure direct model calculations. The top two plots show the fraction of the cross section due to $p_{3/2}(E1)$ and $d_{5/2}(E2)$. The middle plot shows the relative phases between the two $E1$ terms. The lower two plots show the relative phase between the two $E2$ terms and the $p_{3/2}(E1)$ term. The errors shown are statistical (for the relative $E1$ phase the errors are $<4°$).

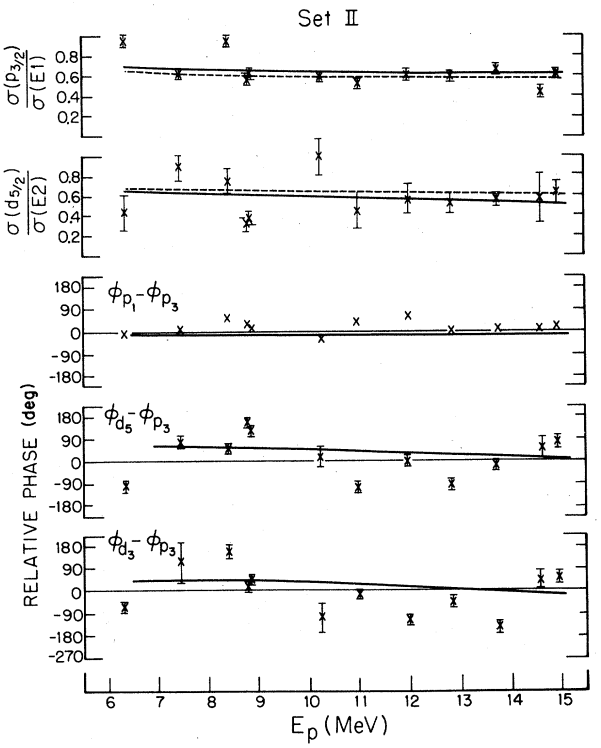

FIG. 7. Same as Fig. 6 but for the solutions with $\sigma(p_{3/2})/\sigma(E1)\approx 0.6$.

The absolute $E2$ cross sections can be deduced from the experimentally determined T-matrix elements by means of the expression

$$\sigma(E2)=4\pi A_0(2d_{3/2}{}^2+3d_{5/2}{}^2),$$

where A_0 is taken from Table I. The results for the solutions of set I (solid dots) and set II (crosses) are shown in Fig. 8. A discussion of

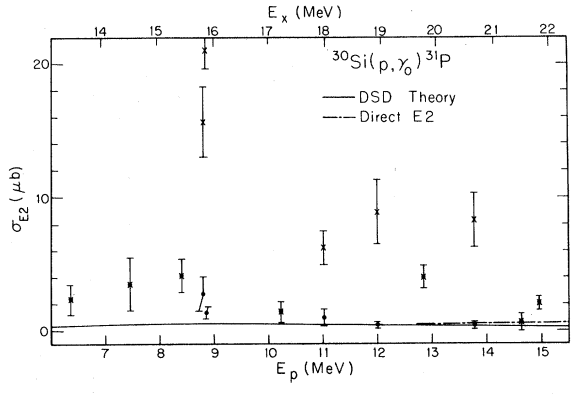

FIG. 8. The angle integrated $E2$ cross section for the ^{30}Si$(p,\gamma_0)^{31}$P reaction. The solid dots represent set I solutions and the crosses set II as described in the text. The solid line is the extended DSD prediction, while the dot-dashed curve is the DSD results with the collective isoscalar quadrupole term ignored.

these data will be given below.

The fact that it is not possible to handle $M1$, E1, and $E2$ radiation at the same time with this type of "model independent" $(\vec{p},\gamma)$ analysis is a limitation of the method and makes it impossible in the present work to rigorously rule out $M1$ effects. To estimate the effects of $M1$ radiation on the extracted values of $\sigma(E2)$, an $M1$ $d_{3/2}$ amplitude and phase was included in the fitting procedure. In all cases the values $\sigma(E2)$ were unchanged or increased.

Because $J^\pi = \frac{3}{2}^+$ for the first excited state of ^{31}P, a T-matrix element analysis of the (p,γ_1) angular distribution data is significantly more complicated than that for the (p,γ_0) case. There are now three $E1$ and five $E2$ complex T-matrix elements which can contribute to the cross section. While the a_k and b_k coefficients have been extracted (Table II), no further analysis has been carried out for this case.

V. $E2$ SUM RULES

The $E2$ cross sections extracted from the data for the ^{30}Si$(\vec{p},\gamma_0)^{31}$P can be used in a comparison with the EWSR. As given by Nathan and Nilsson[28] for $\Delta T = 0$ transitions, the EWSR can be written as

$$\int \frac{\sigma(E2)}{E_\gamma^2}\, dE_\gamma = \frac{\pi^2}{3}\,\frac{e^2}{\hbar c}\,\frac{\langle r_p^2\rangle}{mc^2}\,\frac{Z^2}{A}.$$

The (p,γ_0) $E2$ cross sections shown in Fig. 8 were converted by the method of detailed balance to $\sigma_{E2}(\gamma,p_0)$ and used to estimate the above integral. Two methods were used to determine the experimental values of the integral from $E_x = 12.9$ to 21.9 MeV and the results are listed in Table III. First, it was assumed that $\sigma_{E2}(\gamma,p_0)$ varies smoothly and the integral was approximated by summing a histogram constructed from the experimental points. Second, it was assumed that $\sigma_{E2}(\gamma,p_0)$ fluctuates in a manner similar to $\sigma_{E1}(\gamma,p_0)$ and that the measured $E2$ cross sections are peak values. This second procedure gives smaller values for the integral. The current experiment indicates that the (γ,p_0) channel exhausts from 9 to 13% or from 21 to 31% of the $\Delta T = 0$ $E2$-EWSR for solution sets I and II, respectively. These values are to be compared to about 10% ($E_x = 14$ to 27 MeV) obtained from the ^{14}C$(p,\gamma_0)^{15}$N reaction,[6,7] about 30% ($E_x = 14.6$ to 22.2 MeV) for the ^{13}C$(p,\gamma_1)^{14}$N reaction,[29] and 20 to 30% ($E_x = 13.9$ to 29.0 MeV) for the ^{15}N$(p,\gamma_0)^{16}$O reaction (reported by Snover in Ref. 9). The prediction of the extended DSD model calculation is also presented in Table III.

TABLE III. Summary of the $\Delta T = 0$ $E2$ energy-weighted sum rule obtained by summing the experimental data for $E_x = 12.9$ to 21.9 MeV. The errors are statistical only. Also shown is the value from the DSD calculation. The range given for the percentage of the EWSR is discussed in the text.

	$\int \frac{\sigma dE}{E^2}$ (μb/MeV)	Percent
Set I	2.5 ±0.4	9–13
Set II	6.0 ±0.5	21–31
DSD	0.45	2.3
EWSR [a]	19.2 [a]	

[a] Calculated for $\langle r_p^2\rangle^{1/2} = 3.1$ fm (Ref. 37).

VI. DIRECT-SEMIDIRECT MODEL CALCULATIONS

The DSD capture model[10-12] has recently been extended to include electric quadrupole processes.[7,14,30-32] Calculations based on the DSD model may help in providing a clearer understanding not only of the gross properties of the giant dipole but also of the giant quadrupole resonances. This has been demonstrated in a recent analysis of the ^{40}Ca(n,γ_0) reaction.[33] For a zero spin target, the transition matrix element has the form

$$t^v(p\to\gamma) = \left\langle \phi_{nljm}(x)\middle| d^v(x) + \sum_T \frac{V^v_{1,\tau=1}(x)}{E - E_{11}(T) + \frac{1}{2}i\,\Gamma_{11}(T)}\middle|\chi_i^{(+)}(x)\right\rangle + \left\langle \phi_{nljm}(x)\middle| q^v(x) + \sum_{\tau=0,1} \frac{V^v_{2,\tau}(x)}{E - E_{2\tau} + \frac{1}{2}i\,\Gamma_{2\tau}}\middle|\chi_i^{(+)}(x)\right\rangle,$$

where $|\phi_{nljm}(x)\rangle$ is the single-particle bound state, $|\chi_i^{(+)}(x)\rangle$ the scattering states, and $d^v(x)$ and $q^v(x)$ are the single-particle dipole and quadrupole operators, respectively. The summation index T refers to the two possible isospin components of the GDR which are labeled as $T_<$ and $T_>$. The index τ labels the isoscalar ($\tau = 0$) and isovector ($\tau = 1$) transition operators, the $E1$ strengths being pure isovector. The dipole and quadrupole form factors, $V_1^v(x)$ and $V_2^v(x)$, respectively, appear in the terms which represent the possible presence of the giant dipole and quadrupole resonances. These form factors are a product of the particle-vibration coupling which is responsible for the inelastic excitation of the collective state and the matrix element in the target nucleus which describes the γ decay of the collective state.

The complex dipole coupling interaction of Ref. 12 was used in the calculation. This interaction is proportional to $rU_1(r)$, where $U_1(r)$ is the complex optical-model symmetry potential. The real part V_1 and the imaginary part W_1 were treated as free parameters to fit the 90° cross section and

angular distribution coefficients a_2 and b_2. The coupling interaction for the isoscalar quadrupole semidirect term[14] was taken to have a surface-peaked shape. It is proportional to $-rdU_0(r)/dr$, where $U_0(r)$ is the real central potential ($U_0 = 50$ MeV). For the isovector part, the coupling was taken to have a volume form proportional to $r^2U_1(r)$ ($V_1 = 75$ MeV, $W_1 = 0$). The optical-model parameters of Becchetti and Greenlees[34] were used throughout, and the strength of the bound state potential was adjusted to get the correct binding energy.

As was discussed in Sec. IV A the yield curve for ^{30}Si$(p,\gamma_0)^{31}$P suggests the presence of two broad peaks centered near 17 and 21 MeV. It was, therefore, assumed that the dipole processes proceed via two uncoupled collective dipole excitations which may be associated with $T_<$ and $T_>$. The two resonance energies [$E_{11}(T_<)$ and $E_{11}(T_>)$] were adjusted to fit the experimental (p,γ_0) yield curve after it had been averaged with an energy interval of 1.1 MeV (not shown). The resulting fit is shown in Fig. 2 for the parameters $E_{11}(T_<)/\Gamma_{11} = 17.3/3.4$ and $E_{11}(T_>)/\Gamma_{11} = 20.6/4.0$ MeV, respectively.

The results of calculations which include all dipole and quadrupole terms are shown in Fig. 9 for the a_k and b_k coefficient. The quadrupole parameters are $E_{20}/\Gamma_{20} = 19.7/7.1$ and $E_{21}/\Gamma_{21} = 31/7$ MeV, respectively. The values of the collective quadrupole matrix elements were taken to exhaust 32% and 75% of the EWSR values for the isoscalar and isovector terms, respectively. The isoscalar GQR parameters were taken from Bertrand[4] while those for the isovector GQR are from a separate study in this laboratory of this resonance using the ^{30}Si$(p,\gamma_1)^{31}$P reaction.[35] The proton spectroscopic factor was taken from Endt.[36] The main trends of the data are well reproduced for excitation energies above about 14 MeV. Since the large strength seen in the yield curve for $E_x < 14$ MeV is not accounted for by the calculation, the curves are not shown below this excitation energy. The dotted curves are the result of using the complex form factor for the semidirect dipole terms, while the solid curves show the results for purely real terms ($w_1 = 0$). The dot-dashed curves shown for the odd coefficients are the results of a calculation which used real coupling for the semidirect dipole terms and ignored the isoscalar GQR.

The relative amplitudes and phases calculated with the extended DSD model including all dipole and quadrupole terms are compared with those extracted directly from the experimental data in Figs. 6 and 7. In general there is better agreement for set II for the relative $p_{3/2}$ dipole cross section

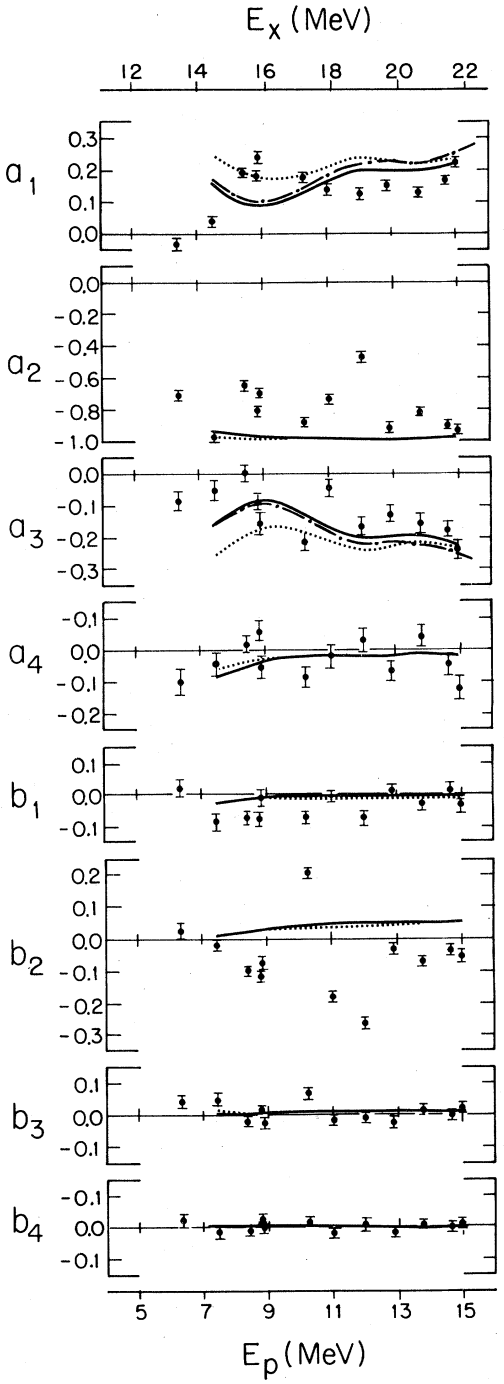

FIG. 9. The a_k and b_k coefficients for the ^{30}Si$(p,\gamma_0)^{31}$P reaction. As discussed in the text, the curves are the results of DSD model calculations with the following conditions: dotted curves—complex dipole form factor, solid curves—real dipole form factor, and dot-dashed curves—real dipole form factor with semidirect isoscalar quadrupole form factor set to zero.

and the relative $d_{5/2}$ quadrupole cross section. The quality of the agreement for the relative dipole phases is similar for both sets I and II. Especially well reproduced are the quadrupole-dipole relative phases $\phi(d_{5/2}) - \phi(p_{3/2})$ for set I. Somewhat worse is the agreement for the $\phi(d_{3/2}) - \phi(p_{3/2})$ relative phases of set I. For set II, both $\phi(d_{5/2})$-$\phi(p_{3/2})$ and $\phi(d_{3/2})$-$\phi(p_{3/2})$ show the general trend of the calculated values, but there are rather large deviations near $E_p \sim 10$ MeV.

Also shown as dashed lines in Figs. 6 and 7 are the results of a pure direct model calculation $[V(x)=0]$ for the relative amplitudes. The results are the same as would be obtained from the simple DSD model as developed by Brown[10] using the schematic model $[V(x) \propto r^L]$. The most striking feature of the calculations is the stability of the predicted relative amplitudes to substantial changes in the semidirect form factors.

The $E2$ cross section obtained from the extended DSD calculation is shown in Fig. 8 as a solid curve and exhausts 2.3% of the $\Delta T=0$ $E2$ EWSR. This calculated cross section is due almost completely to direct $E2$ capture. Above $E_x \sim 16$ MeV, there is some agreement between the DSD calculations and solution set I, while below 16 MeV the experimental values of $\sigma(E2)$ lie well above the curve. On the other hand, there is no agreement between solution set II and the calculation.

On the basis of a comparison of the magnitudes of the relative $E1$ amplitudes with the results of the DSD calculations, solution set II appears to be the physical solution. The validity of this conclusion receives support from previous studies which have shown that the DSD calculation can reliably predict this feature of the data. Furthermore, as has already been pointed out, for the case of ^{30}Si$(p,\gamma_0)^{31}$P and in the absence of abnormally strong spin-orbit effects, $\sigma(p_{3/2})/\sigma(E1)$ must be near $\frac{2}{3}$ [and $\sigma(d_{5/2})/\sigma(E2)$ near $\frac{3}{5}$] regardless of the form factor used in the DSD model calculations. These results imply that the larger $E2$ solution (the x's) of Fig. 8 are the physical ones. While this choice of solutions appears to be preferred, it should be emphasized that solution set I cannot be absolutely ruled out.

VII. CONCLUSIONS

The ^{30}Si$(p,\gamma_0)^{31}$P and ^{30}Si$(p,\gamma_1)^{31}$P$(E_x=1.27$ MeV) reactions have been studied with polarized protons over the excitation region of the giant dipole resonance of ^{31}P. For the (p,γ_0) reaction, the relative amplitudes and phases of the two $E1$ and two $E2$ T-matrix elements have been determined under the assumption that the effects of $M1$ radiation are negligible.

The $E1$ solutions show three cases—two which are predominantly $p_{3/2}$ proton capture and one which is predominantly $p_{1/2}$ proton capture. The DSD model calculations suggest that the case with $\sigma(p_{3/2})$ accounting for about 60% of the $E1$ cross section is the physical solution. The $E2$ cross section associated with this latter case accounts for from 21 to 31% of the $E2$ $\Delta T=0$ EWSR for $E_x=12.9$ to 21.9 MeV. This large $E2$ strength is in disagreement with the results of the extended DSD model calculations which predict an $E2$ cross section in the ground state channel of 2.3% of the $\Delta T=0$ EWSR and a smooth energy dependence. The main experimental $E2$ strength is observed in the region of $E_x \approx 15$ to 21 MeV which is somewhat lower than the expected excitation energy of the GQR obtained from the equation $63/A^{1/3}=20$ MeV. This is the same as the trend observed by Kiss *et al.*[38] and Knöpfle *et al.*,[39] who studied the GR region of sd-shell nuclei by inelastic scattering of α particles. However, before the $E2$ strength observed in this experiment can be identified with the GQR, more measurements are needed, especially for the excitation energy region above 22 MeV, to confirm that $\sigma(E2)$ has the proper energy dependence. This is especially true in view of the fact that the proton capture cross section can be a mixture of isoscalar and isovector strength.

*On leave from Institute Josef Stefan, University of Ljubljana, Ljubljana, Yugoslavia.

[1]H. F. Glavish, S. S. Hanna, R. Avida, R. N. Boyd, C. C. Chang, and E. Diener, Phys. Rev. Lett. 28, 766 (1972).
[2]S. S. Hanna, H. F. Glavish, E. M. Diener, J. R. Calarco, C. C. Chang, R. Avida, and R. N. Boyd, Phys. Lett. 40B, 631 (1972).
[3]H. R. Weller, N. R. Roberson, and S. R. Cotanch, Phys. Rev. C 18, 65 (1978).
[4]F. E. Bertrand, Annu. Rev. Nucl. Sci. 26, 457 (1976).
[5]H. F. Glavish, in *Proceedings of the Fifth Symposium on the Structure of Low-Medium Mass Nuclei*, edited by J. P. Davidson and B. D. Kern (The University Press of Kentucky, Lexington, Kentucky, 1973), p. 233.
[6]H. R. Weller, R. A. Blue, N. R. Roberson, D. G. Rickel, S. Maripuu, C. P. Cameron, R. D. Ledford, and D. R. Tilley, Phys. Rev. C 13, 922 (1976).
[7]K. A. Snover, J. E. Bussoletti, K. Ebisawa, T. A. Trainor, and A. B. McDonald, Phys. Rev. Lett. 37, 273 (1976).
[8]S. S. Hanna, H. F. Glavish, R. Avido, J. R. Calcaro,

E. Kuhlmann, and R. LaCanna, Phys. Rev. Lett. 32, 114 (1974).
[9]K. A. Snover, in *Proceedings of the Third International Symposium on Neutron Capture Gamma-Ray Spectroscopy an Related Topics*, edited by Robert Chrien (Plenum, New York, 1979), and K. A. Snover, in Proceedings of the Giant Multipole Resonance Topical Conference, edited by F. E. Bertrand (unpublished).
[10]G. E. Brown, Nucl. Phys. 57, 339 (1964).
[11]C. F. Clement, A. M. Lane, and J. A. Rook, Nucl. Phys. 66, 273 (1965).
[12]M. Potokar, Phys. Lett. 46B, 346 (1973).
[13]K. T. Knöpfle, G. J. Wagner, P. Paul, H. Brewer, C. Mayer-Böricke, M. Rogge, and P. Turek, Phys. Lett. 74B, 191 (1978).
[14]M. Potokar, Stanford University Progress Report 1977 (unpublished), p. 99 and (unpublished).
[15]J. D. Turner, C. P. Cameron, N. R. Roberson, H. R. Weller, and D. R. Tilley, Phys. Rev. C 17, 1853 (1978).
[16]D. M. Skopik, H. R. Weller, N. R. Roberson, and S. A. Wender, Phys. Rev. C 19, 601 (1979).
[17]T. A. Trainer, T. B. Clegg, and P. W. Lisowski, Nucl. Phys. A220, 533 (1974).
[18]A. Landsdorf, in *Fast Neutron Physics*, edited by J. B. Marion and J. L. Fowler (Interscience, New York, 1960), p. 744.
[19]D. M. Brink, thesis, Clarendon Laboratory, University of Oxford, 1955.
[20]W. Gellie, K. H. Lokan, and N. K. Sherman, in *Proceedings of the International Conference on Photonuclear Reactions and Applications*, edited by B. L. Berman (Lawrence Livermore Laboratory, University of California, 1973), p. 171.
[21]A. Veyssiere, H. Beil, R. Bergere, P. Carlos, A. Lepretre, and A. de Miniac, Nucl. Phys. A227, 513 (1974).
[22]See, for example, E. Hayward, National Bureau of Standards Monograph 118 (U.S. Department of Commerce, 1976), p. 38.
[23]R. O. Akyuz and S. Fallieros, Phys. Rev. Lett. 27, 1016 (1971).
[24]P. Paul, in *Proceedings of the International Conference on Photonuclear Reactions and Applications Asilomar*, edited by B. L. Berman (Lawrence Livermore Laboratory, University of California, 1973), p. 407.
[25]E. D. Arthur, D. M. Drake, and I. Halpern, Phys. Rev. Lett. 34, 914 (1974).
[26]S. S. Hanna, in *Proceedings of the International Conference on Nuclear Structure and Spectroscopy*, Vol. 2, edited by H. P. Blok and A. E. L. Dieperink (Scholar's Press, Amsterdam, The Netherlands, 1974), p. 249, and reference therein.
[27]H. H. Rosenbrock, Comput. J. 3, 175 (1960).
[28]O. Nathan and S. G. Nilsson, in *Alpha-, Beta- and Gamma-Ray Spectroscopy*, edited by K. Siegbahn (North-Holland, Amsterdam, 1965), pp. 601–700.
[29]J. D. Turner *et al.*, Phys. Rev. C 21, 525 (1980); J. D. Turner, Ph.D. thesis, Duke University, 1978 (unpublished).
[30]G. Longo *et al.*, Phys. Lett. 65B, 15 (1976).
[31]G. Longo *et al.*, Phys. Lett. 76B, 15 (1978).
[32]H. Kitazawa and Nobakiro Yamamuro, J. Phys. Soc. Jpn. 41, 1102 (1976).
[33]S. A. Wender, N. R. Roberson, M. Potokar, H. R. Weller, and D. R. Tilley, Phys. Rev. Lett. 41, 1217 (1978).
[34]F. B. Becchetti, Jr. and G. W. Greenlees, Phys. Rev. 182, 1190 (1969).
[35]C. P. Cameron, Ph.D. thesis, Duke University, 1977 (unpublished).
[36]P. M. Endt, At. Data Nucl. Data Tables 19, 23 (1977).
[37]C. W. de Jager, H. de Vries, and C. de Vries, At. Data Nucl. Data Tables 14, 479 (1974).
[38]A. Kiss *et al.*, Phys. Rev. Lett. 37, 1188 (1976).
[39]K. T. Knöpfle *et al.*, Lecture Notes in Physics 92, 443 (1979).